Characteristic mode analysis of planar dipole antennas

Aliakbari Abar, Hanieh; Lau, Buon Kiong

Published in:
2019 13th European Conference on Antennas and Propagation (EuCAP)

2019

Document Version:
Peer reviewed version (aka post-print)

Characteristic Mode Analysis of Planar Dipole Antennas

Hanieh Aliakbari, Buon Kiong Lau
Department of Electrical and Information Technology, Lund University, Lund, Sweden, hanieh.aliakbari_abar@eit.lth.se

***Abstract*—Planar monopole antennas are popular due to their attractive properties, but their operating mechanisms are still not well understood. Based on image theory, planar monopoles can be analyzed using their dipole counterparts. Here, the bandwidth and radiation pattern of planar dipoles is studied in detail using characteristic mode analysis for different design parameters. The results show that insignificant modes can help to improve the bandwidth without contributing to the radiation property. Moreover, a tradeoff is observed between pattern stability and impedance bandwidth as the dipole width varies. Furthermore, it is found that an offset in the feed point leads to a degradation in both the modal and impedance bandwidths.**

***Index Terms*—Characteristic mode analysis, planar dipole antenna, impedance bandwidth, wideband antenna.**

I. INTRODUCTION

Nowadays, it is desirable to increase the number of operating frequencies covered by the antennas in different wireless applications. This need for increasing bandwidth is especially challenging when the antennas should be small and at the same time facilitate pattern stability.

Planar rectangular monopole antennas are commonly proposed for wireless communications, due to its wideband characteristic, near omnidirectional radiation patterns and simple structures [1]-[5]. In [1], the basic square planar monopole (with center feed) on a large ground plane provides an impedance bandwidth ratio (VSWR < 2) of 1:2.1. A beveled version of this basic design is shown to improve the impedance matching such that the bandwidth ratio can be as large as 1:5.75 [2]. Moreover, it is shown in [3] that by folding the two edges of a planar rectangular monopole by ±90°, an improved radiation pattern can be realized at the cost of a lower bandwidth ratio of 1:3. Other studies in [4] and [5] reveal that increasing the number of square monopole feed points increases the impedance bandwidth to 1:5.3 and 1:8.3, respectively.

In [6], characteristic mode analysis (CMA) [7] is carried out on a *quasi*-planar monopole with a small coplanar ground plane, which is unlike the monopoles in [1]-[5] where the ground planes are perpendicular to the planar radiators. It is found that the modes of the radiator and the small ground plane in [6] both contribute to an improved bandwidth. However, existing studies do not offer detailed analysis of the operating mechanism of monopole antennas that do not rely on ground plane modes for radiation in the band of interest. Moreover, if the ground plane is large enough so that it does not contribute significantly to the antenna radiation, the monopole structure can be studied as a planar dipole antenna by applying the image theory.

In this context, this paper performs a parametric study of the basic form of planar dipole antennas using CMA [7], to gain insights into the physical mechanisms that give rise to the achieved bandwidth of wideband monopoles, as well as how they affect the radiation pattern. Unlike conventional CMA [7], where no assumption is made on the location of the excitation source, this study focuses on the modal behavior for the center-feed design.

This paper is organized as follows: CMA as applied in this paper is briefly reviewed in Section II. The characteristic modes (CMs) of a rectangular perfect electric conductor (PEC) plate is also presented as a reference case. Section III concerns the study of planar dipole bandwidth using CMA, based on which the bandwidth and pattern properties are investigated for the center feed position in Section IV. Section V looks into the effects of offset in the feed position. The results reveal that, for the single-feed designs considered in this work, the bandwidth is in fact optimized for the center feed position. Finally, a conclusion is given in Section VI.

II. CHARACTERISTIC MODE ANALYSIS

A. Parameters for CMA

The parameters of interest for CMA in this work are both excitation-independent ones (i.e., characteristic eigenvalues, characteristic currents and far-fields) as well as excitation-dependent ones (modal weighting coefficient, modal input admittance). Here, the modal input admittance parameter is reviewed [8], as it is less common than the other parameters that are typically found in CM literature, e.g., [7].

CMs modes are defined as real-valued current modes that reside on the surface of a PEC body, which depend on its shape and size, and independent of excitation [7]. When an excitation source is added to the PEC body, the surface current density (i.e., J) can be expanded as

$$J = \sum_{n=1}^{\infty} \underbrace{\left[V_n / \left(1 + j\lambda_n\right) \right]}_{\alpha_n} J_n \qquad (1)$$

where λ_n and J_n are the characteristic eigenvalue and current of mode n. α_n is the modal weighting coefficient. V_n is the modal excitation coefficient which is calculated by the inner product of the characteristic current and excitation $\langle J_n^*, E_{\tan} \rangle$, where $E_{\tan}$ is the tangential surface current produced by the excitation and * denotes the complex conjugate operator.

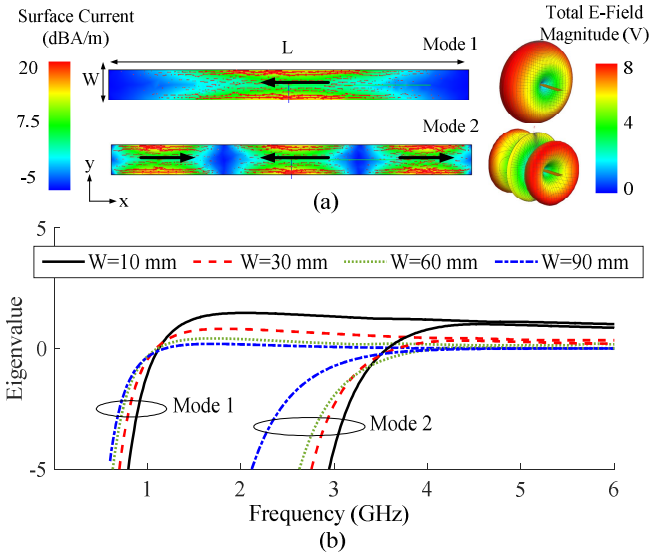

Fig. 1. (a) First two modes of a narrow rectangular plate (L = 120 mm, W = 10 mm) with maximum currents in the center at resonant frequency, and (b) eigenvalues of the corresponding modes in rectangular plates with different widths and L = 120 mm, up to 6 GHz.

Then, the input admittance of an antenna can be obtained from the current I_{in} and voltage V_{in} at the feeding port as [8]

$$Y_{in} = \frac{I_{in}}{V_{in}} = \sum_{n=1}^{\infty} \alpha_n J_n^p \Big/ E_{in}^p = \sum_{n=1}^{\infty} \left(J_n^p\right)^2 \Big/ \left(1 + j\lambda_n\right) = \sum_{n=1}^{\infty} Y_{in}^n \quad (2)$$

where J_n^p and E_{in}^p are the currents (of mode n) and electric field at the feeding port, respectively. Y_{in}^n is the input admittance for mode n, which can be used to evaluate the contribution of mode n to impedance matching. Finally, the modal reflection coefficient (of mode n) is given by [8]

$$\Gamma_n = \left(1/Y_{in}^n - Z_0\right) \Big/ \left(1/Y_{in}^n + Z_0\right) \quad (3)$$

B. *CMA of rectangular PEC plate*

The CMs of infinitely thin rectangular conducting plates of dimensions $L \times W$ (length × width) were obtained from the method of moments (MoM) solver of Altair FEKO 2018. In this example, L = 120 mm and W varied from 10 mm to 90 mm. The eigenvalues of half-wave and 3/2-wave dipole modes of the rectangular plate are presented in Fig. 1 as modes 1 and 2. These modes were identified from their current distributions, as shown in Fig. 1(a) for the case of W = 10 mm. These two modes can be directly compared to the first two modes that can be efficiently excited by center feed dipoles (half-wave and 3/2-wave dipole modes). The results are used as reference cases for the CMA of planar dipoles.

As can be seen in Fig. 1(b), as the width increases (for a given length), the fundamental (half-wave) dipole mode contributes to the radiation more efficiently, if excited. In fact, the eigenvalue stays small ($|\lambda| \le 1$) after the resonant frequency ($\lambda = 0$) for $W \ge 30$ mm. This indicates that in theory there is no limitation in the modal bandwidth of this mode, which facilitates wideband designs. The characteristic currents of mode 1 (at resonance) for wider rectangular plate

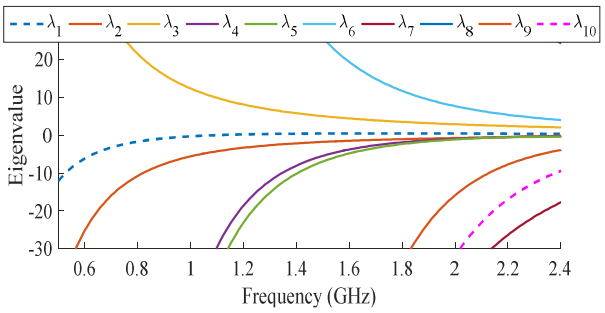

Fig. 2. The eigenvalues for the first 10 CMs of the rectangular plate with W = 60 mm and L = 120mm.

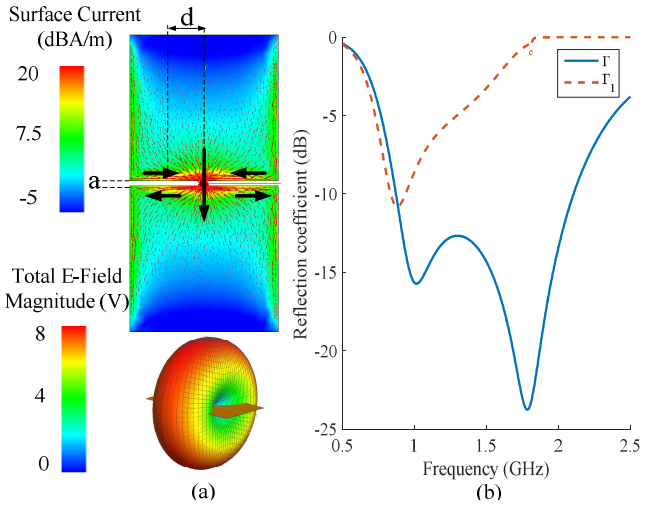

Fig. 3. (a) Current distribution and far-field pattern of the fundamental mode at its resonant frequency, (b) total (Γ) and mode 1 (Γ_1) reflection coefficents over frequency (d = 0 mm, W = 60 mm, a = 2 mm).

(W > 10 mm) shows similar trends to Fig. 1(a), in that the maximum currents are located at the two edges along the length, weaker between the two edges and weakest at the two ends. To illustrate that many other modes become more significant as W increases, the eigenvalues of the first 10 CMs of a rectangular plate over 0.5–2.3 GHz are shown in Fig. 2 for W = 60 mm. To ensure reliable mode tracking the CMA was done with 2 MHz interval. In this case, mode 2 (3/2-wave dipole mode) in Fig. 1(b) corresponds to mode 10 in this figure.

III. CMA OF DIPOLE ANTENNA

Compared to the solid rectangular plate in the previous section, for dipole shape a narrow slot of width a is added in the middle of the longer side along with a shorting strip across the slot (modeling the gap feed) at an offset distance d from the slot center (see Fig. 3(a) for d=0). In this section, no offset is considered, i.e., d = 0. It is noteworthy that, contrary to the fundamental mode current of the rectangular plate in Fig. 1(a), the current of the first mode in the dipole, as shown in Fig. 3(a), is maximum in the shorting strip, and some currents flow along the slot direction in addition to the currents along the length. Although the modal currents are

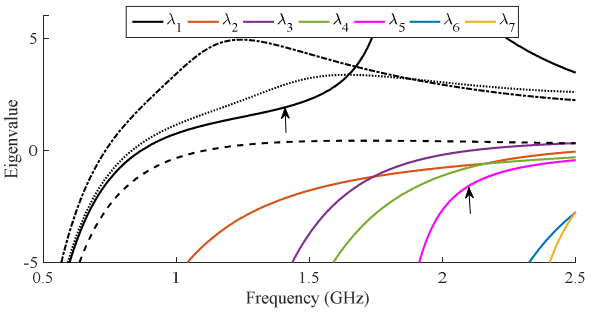

Fig. 4. First seven eigenvalues of the dipole with $d = 0$ (solid lines); mode 1's eigenvalue of the dipole with $d = W/4$ (in dotted line), and $d = W/2$ (in dot-dashed line) and solid plate (dashed line). Here L=120 mm, W=60 mm and a=2 mm. The two arrows point to the modes that contributes more to the dipole bandwidth.

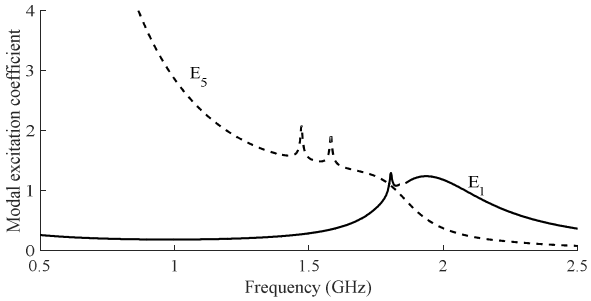

Fig. 5. Modal excitation coefficient of the two most significant modes out of the first seven modes for $d = 0$, L=120 mm, W=60 mm and a=2 mm.

different in Fig. 1(a) and Fig. 3(a), the far-field patterns of the fundamental mode in both cases are similar at the resonant frequency, due to the currents on the two sides of the slot are in opposite directions and they cancel each other in the far-field.

From the above discussions, a planar dipole is expected to efficiently excite the fundamental mode, as having a voltage gap source instead of the shorting strip feeds this mode at its maximum current region. In addition, the simple feed may also excite other resonant or near-resonant modes that have high currents in this region. Therefore, the relatively large 6 dB impedance bandwidth of the gap feeding port of 0.8-2.3 GHz, as depicted in Fig. 3(b), may at first be attributed to mode 1 and possibly other modes. In fact, by computing the reflection coefficient due to mode 1 (i.e., Γ_1) using (3) and presenting the result in Fig. 3(b), it can be seen that mode 1 only contributes to the bandwidth at the lower frequencies. However, this behavior is consistent to the small modal bandwidth of this mode, as can be deduced from its rather steep eigenvalue curve in Fig. 4.

To examine the contribution of other modes, Fig. 4 also shows six additional modes with eigenvalue magnitude $|\lambda_n| \leq 5$. Moreover, the eigenvalue of mode 1 of the solid plate is added to Fig. 4 (dashed line) for the sake of comparison. It is observed that the resonant frequency of the dipole is lower than the solid plate (i.e., 0.8 vs. 1.1 GHz). Moreover, Fig. 4 shows that the modal bandwidth of the fundamental mode is

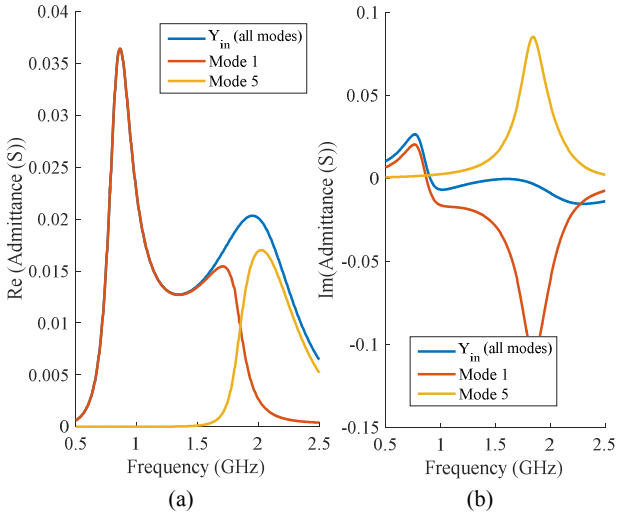

Fig. 6. Total and modal (a) Re(admittance) and (b) Im(admittance) of the planar dipole.

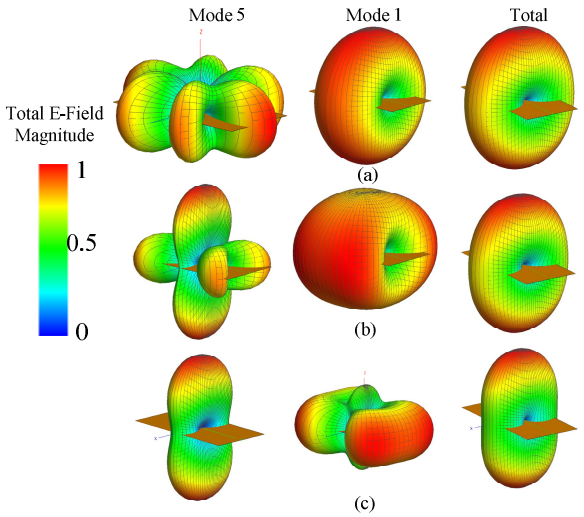

Fig. 7. Normalized electric far- field patterns for $d = 0$ at: (a) 1.5 GHz, (b) 1.8 GHz and (c) 2.3 GHz.

very much smaller than that of the solid plate. In contrast, the eigenvalue curves of modes 2-7 appear flatter as they approach their respective resonant frequencies (outside the plot); however, their resonances are at higher frequencies than the dipole bandwidth of Fig. 3(b) and hence they are considered as less significant modes. It is noted that mode 10 in Fig. 2 can be equated to mode 5 in Fig. 4, as they share similar current distribution.

On the other hand, the modal excitation coefficients V_n of the first 7 modes were obtained from Altair FEKO and presented in Fig. 5. It can be seen that modes 1 and 5 are both excited within the dipole bandwidth. Therefore, it is conceivable that mode 5 can contribute to the dipole bandwidth despite being a less significant mode, since the modal weighting coefficient α_n depends on both factors. To verify the role of mode 5, modal admittances are plotted in Fig. 6 together with the total admittance. Based on Fig. 6(a),

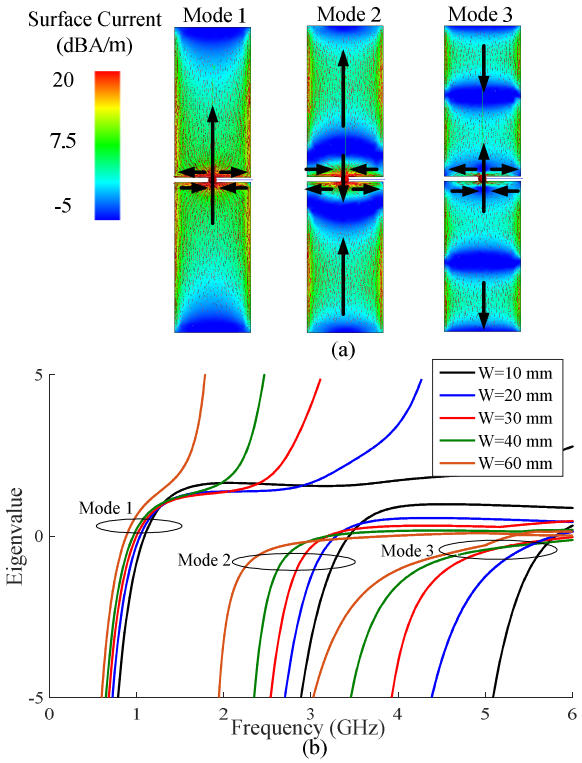

Fig. 8. Case of L = 120 mm, a = 2 mm and d = 0: (a) First three significant modes for W = 30 mm, (b) eigenvalues for different widths over frequency.

it can be seen that the antenna radiation resistance over 0.7–1.8 GHz is determined mainly by mode 1. However, mode 1's reflection coefficient between 1 and 2.3 GHz is inferior to the total reflection coefficient in Fig. 3(b). The better total reflection coefficient is resulted mainly from the interaction of net capacitive and inductive energies stored by mode 1 and the less significant mode 5 plotted in Fig. 6(b), which leads to low total stored energy and low total reflection coefficient in 0.8-2.3 GHz. Mode 5 has negligible role in radiation (i.e., small α_n) up to 1.8 GHz and its maximum contribution to the dipole radiation is at 2.1 GHz. However, it has an effect on the input impedance (i.e., reactance) below 2.1 GHz, as shown in Fig. 3(b) based on (2). Based on (2), the admittance of mode n is can be expressed as real and imaginary parts as follows

$$Y_{in}^{n} = \left(1 - j\lambda_n\right)\left(J_n^p\right)^2 \Big/ \left(1 + \lambda_n^2\right). \tag{4}$$

This expression shows that the imaginary part of the admittance is less dependent on the modal eigenvalue as compared to the real part.

Finally, Fig. 7 plots the modal and total patterns within the dipole bandwidth. It shows that the patterns of modes 1 and 5 evolve substantially in frequency. However, the total pattern is relatively stable, retaining the "donut shape", albeit becoming slightly distorted at higher frequencies.

IV. CMA of Varying Planar Dipole Width

The influence of the planar dipole's form factor (length vs. width) on bandwidth and far-field pattern is studied in this section. Similar to the previous section, L = 120 mm and

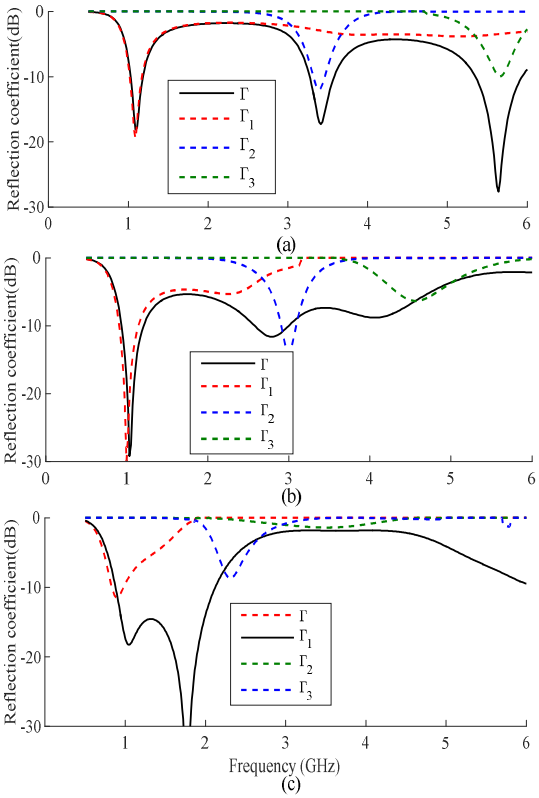

Fig. 9. Total and modal reflection coefficients of the dipole without matching circuit for: (a) W = 10 mm, (b) W = 30 mm, (c) W = 60 mm.

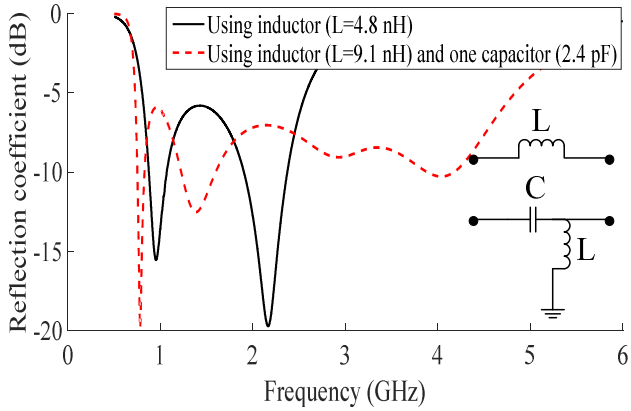

Fig. 10. Reflection coefficients of the dipole with matching circuit for W = 30 mm.

a = 2 mm, and center feed dipole (d = 0) is considered. Fig. 8(a) shows the currents of the first three significant modes for W = 30 mm, which are similar in distribution for other considered widths. Mode 1 in Fig. 8(a) is the fundamental mode, whereas modes 2 and 3 are higher-order modes. The number of significant modes increase gradually with frequency. The eigenvalue curves of the three significant modes in Fig. 8(b) are plotted for W varying from 10 mm to 60 mm. When W is small, the fundamental mode has larger modal bandwidth and higher resonant frequency than larger W. For a smaller W, the pattern retains its dipole shape until a higher frequency, leading to the pattern being stable over a

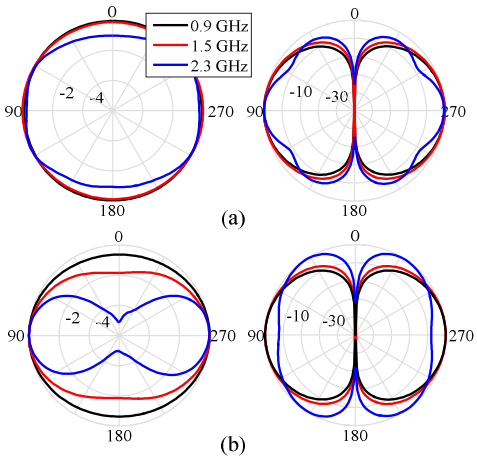

Fig. 11. Normalized E-plane (right) and H-plane (left) electric far-field patterns for: (a) W = 30 mm, (b) W = 60 mm.

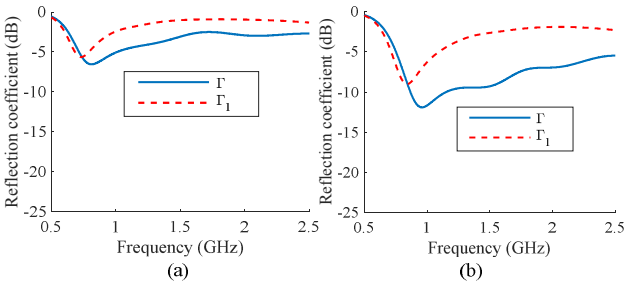

Fig. 12. Total and mode 1 reflection coefficients of the dipole with L = 120 mm, a = 2 mm and W = 60 mm for: (a) $d = W/2$, (b) $d = W/4$.

larger bandwidth. On the other hand, if matching circuit is not used (as in the previous section), the dipole bandwidth and matching will be worse in the lower frequencies as W decreases (see Fig. 9). So there exists a trade-off between pattern stability and impedance bandwidth for different widths.

If a one-element matching circuit is used, a slightly larger impedance bandwidth is achieved with a smaller width (e.g., 30 mm) than the case of W = 60 mm without matching circuit in Fig. 9(c), and it offers more stable pattern over the entire bandwidth. As shown in Fig. 10, the bandwidth of 0.8-2.5 GHz is obtained with only one inductor and 0.7-4.7 GHz with two-element matching. In the latter case, the pattern starts to deviate from the dipole shape after 2.6 GHz because of the limited bandwidth of mode 1 and the effect of the higher order modes. In order to realize the same bandwidth for W < 30 mm, more complex matching circuits with more than five elements should be used. Fig. 11 shows the patterns for two different W's, where the pattern is more stable for the smaller W. Therefore, it is concluded that both bandwidth and pattern stability are optimized at W = 30 mm with one-element matching.

V. CMA of Varying Dipole Feed Position

The feed position has a strong impact on the dipole bandwidth. Figures 3(b) and 12 show that offsetting the feed position from d = 0 towards $d = W/2$ causes the impedance bandwidth to decrease and to be increasingly dominated by mode 1. This is mainly because only mode 1 is efficiently excited as the offset increases, instead of two modes. It is noted that the small difference between the total and mode 1 reflection coefficients (in Fig. 12(a)) is the result of partial excitation of two less significant modes (modes 3 and 4 in Fig. 4). Apart from single-mode excitation, mode 1 also has a smaller modal bandwidth for d=W/2 offset case, as depicted by its steeper eigenvalue curve in Fig. 5 (dot-dashed line), which indicates a smaller impedance bandwidth.

VI. Conclusion

Using CMA, wideband planar monopoles are studied in this work using their dipole counterparts. It is shown that less significant modes can significantly contribute to bandwidth improvement. Moreover, a trade-off between pattern stability and bandwidth is observed for varying dipole widths. A parameter study of the feed location reveals that proper modal excitation and impedance matching are both critical for antenna performance. Finally, the scope of the analysis is limited to single-feed designs. The analysis of multi-feed designs (e.g., [4]) that offer even larger bandwidths is an interesting subject for future work.

Acknowledgment

This work was supported Swedish Research Council under grants no. 2010-468 and 2016-0468.

References

[1] N. P. Agrawall, G. Kumar, and K. P. Ray, "Wide-band planar monopole antennas," *IEEE Trans Antennas Propag.*, vol. 46, no. 2, Feb. 1998.

[2] M. J. Ammann, "Control of the imprdance bandwidth of wideband planar monopole antennas using a beveling technique," *Microw. Opt. Technol. Lett.*, vol. 30, no. 4, pp. 229-232, Aug. 2001.

[3] K. L. Wong, S. W. Su, and C. L. Tang, "Broadband omnidirectional metal-plate monopole antenna," *IEEE Trans. Antennas Propag.*, vol. 53, no. 1, pp. 581–583, Jan. 2005.

[4] E. Antonino-Daviu, M. Cabedo-Fabres, M. Ferrando-Bataller, and A. Valero-Nogueira, "Wideband double-fed planar monopole antennas," *Electron. Lett.*, vol. 39, no. 23, pp. 1635–1636, Nov. 2003.

[5] K. L. Wong, C. Wu, and S. Su, "Ultrawide-band square planar metal-plate monopole antenna with a trident-shaped feeding strip," *IEEE Trans. Antennas Propag.*, vol. 53, no. 4, pp. 1262–1269, Apr. 2005.

[6] W. Wu and Y. P. Zhang, "Analysis of ultra-wideband printed planar quasi-monopole antennas using the theory of characteristic modes," *IEEE Antennas Propag. Mag.*, vol. 52, no. 6, pp. 67–77, Dec. 2010.

[7] R. F. Harrington and J. R. Mautz, "Theory of characteristic modes for conducting bodies," *IEEE Trans. Antennas Propag.*, vol. 5, pp. 622-628, Sept. 1971.

[8] Q. Zhang and Y. Gao, "Compact low-profile UWB antenna with characteristic mode analysis for UHF TV white space devices," *IET Microw. Antenna Propag.*, vol. 11, no. 11, pp. 1629-1635, Aug. 2017.